

## AN INVESTIGATION OF CONVECTIVE COOLING OF AN ARRAY OF CHANNEL-MOUNTED OBSTACLES

Yong Zeng and Kambiz Vafai

Department of Mechanical Engineering, University of California Riverside,  
Riverside, California, USA

*A numerical investigation of forced convective cooling of an array of obstacles was performed to synthesize the effects of various pertinent parameters on the cooling performance. Reynolds number, channel clearance height-to-element length ratio, spacing-to-channel height ratio, geometric ratio of the blocks, and total number of obstacles were varied to estimate their influence on the cooling process. Two generalized sets of Nusselt number correlations were developed for the obstacles in the channel based on a very large number of computational simulations. The numerical data match the correlation equations quite well.*

### 1. INTRODUCTION

Models for cooling of electronic components have been studied both numerically and experimentally by various investigators. In most of these investigations, the problem is idealized to the fluid flow and thermal analysis of heat generating obstacles, representing the electronic devices, within a channel [1–14]. This description of the problem provides a pathway for obtaining pertinent results. Thermal management is an important issue in the design of electronic devices with an increased power density and shrinking system size. The malfunction of electronic devices is mainly related to the operating temperature distribution and local hot spots [15]. In some cases, this forces a trade off between the devices' performance and reduced liability due to an undesirable operating temperature.

Forced convective heat transfer from a wall-mounted array of obstacles within two parallel plates has been traditionally utilized as a suitable representation of the electronic cooling of the multiple chips placed on a circuit board. The flow passing over the multiple obstacles presents several complexities such as impingement, cavity vortices, and recirculation zone reattachment [4–7]. The convective heat transfer from the surfaces of these obstacles varies substantially with the geometrical configurations of the chips. Periodic boundary conditions are established after the flow passes over several obstacles.

Received 19 February 2009; accepted 19 April 2009.

Address correspondence to Kambiz Vafai, Department of Mechanical Engineering, University of California Riverside, A363 Bourns Hall, Riverside, CA 92521-0425, USA. E-mail: vafai@engr.ucr.edu

### NOMENCLATURE

$D_h$ hydraulic diameter $h$ obstacle height $h_c$ convective heat transfer coefficient $H$ channel height $k$ thermal conductivity $L$ length $n$ normal vector $Nu$ Nusselt number $p$ pressure $Pe_H$ Peclet number $Pr$ Prandtl number $q$ heat flux $\dot{q}$ volumetric heat generation rate $Re_H$ Reynolds number $s$ obstacle spacing $T$ temperature $u$ $x$ -component of velocity $v$ $y$ -component of velocity	$w$ obstacle width $\mu$ dynamic viscosity $\Theta$ dimensionless temperature $\rho$ density  <b>Subscripts</b> $f$ fluid $e$ entrance $L$ left surface $m$ mean $o$ outlet $R$ right surface $s$ solid $T$ top surface $w$ wall $x$ local  <b>Superscripts</b> $*$ dimensionless
---	---

An experimental study was undertaken by Garimella and Eibeck [2] to investigate conditions that trigger a laminar-to-turbulent transition in a channel with mounted elements, the contribution of buoyancy to the total heat transfer, the appropriate characteristic dimensions to be used for nondimensionalization, and the extent of heat transfer enhancement from staggered arrays compared to an inline array. Morris and Garimella [3] developed empirical correlations, which are applicable for single-phase forced-convective heat transfer from inline arrays of three-dimensional heat sources in channels. Their proposed correlations are based on the data from many experiments using air, water, and FC-77 as coolants. Predictions from their proposed correlations differ from the experimental data by an average error of  $\pm 9.4\%$  and a standard deviation of 10%.

An experimental investigation of the forced convective heat transfer from an individual obstacle and arrays of multiple two-dimensional obstacles is given by Young and Vafai [4]. The test channel had a length of 2.5 m with a 1.7 m entrance length. Flow channel height range of  $H=10$  to 90 mm was used. The range of Reynolds numbers established varied from 800 to 13,000, while the heat flux was varied in a range of 950 to 20,200 W/m<sup>2</sup>. Both single as well as a variety of multiple obstacle arrangements were investigated, and a numerical analysis was also performed. The experimental data matched well with the numerical predictions. The experiments using four obstacles of identical streamwise length but with one taller than the other three suggested that the proper placement of a geometrically dissimilar obstacle may passively enhance the heat transfer for critical components.

An extensive investigation of the fluid flow and heat transfer in a parallel plate channel with a single obstacle was conducted by Young and Vafai [5]. By changing the Reynolds number, solid conductivity, heating methods, and pertinent geometrical parameters, the Nusselt number dependence was documented. Increasing the Reynolds number resulted in increasing the strength of the downstream recirculation zone.

In another comprehensive study by Young and Vafai [6], the effects of variations in the obstacles height, width, spacing, number of obstacles, obstacle thermal conductivity, fluid flow rate, and heating methods were thoroughly investigated to illustrate important fundamental and practical results. It was shown that as the Reynolds number increases from 200 to 2,000, the downstream recirculation zone expands axially and gains strength. This downstream recirculation resulted in the largest Nusselt number at the last obstacle's right face. As expected, increasing the thermal conductivity of the obstacles reduced the temperatures and thermal gradients within the obstacles. The obstacles became isothermal when the value of thermal conductivity ratio exceeded 100. Two basic heating methods were explored in their work. These were heating the obstacles from the bottom surface and uniform volumetric heat generation within the obstacles. It was established that the heating methods had a small effect on the Nusselt number. However, geometric variations in the obstacles such as spacing size and shape had a substantial effect on the flow field including the mixing within the cavity spacing between the obstacles resulting in a significant effect on the Nusselt number. The Nusselt number, as well as temperature and velocity periodicity, appeared within a 10 obstacles array over a Reynolds number range of 200 to 2,000.

Investigations given in Young and Vafai [4–6] have established a comprehensive blueprint for various fundamental effects, such as variations in geometrical and thermophysical parameters. The objective of this work is to provide an exhaustive correlation that will capture various pertinent geometrical variations for a large enough set of obstacles for a periodicity formation [6]. This correlation will incorporate and capture all the pertinent geometrical variations over a wide range of Reynolds numbers.

## 2. MODEL CONFIGURATION AND GOVERNING EQUATIONS

The configuration which is analyzed in this work is shown in Figure 1. The distance between the upper and lower wall is  $H$ . Multiple obstacles of width  $w$ , height  $h$ , and space  $s$  between them are considered in this work. At the bottom surface of each obstacle, a heat flux  $q$ , is imposed. The flow is considered to be Newtonian, incompressible, steady-state, and laminar. The buoyancy effects are considered to be negligible. The governing equations for mass, momentum, and energy equations are

$$\frac{\partial u^*}{\partial x^*} + \frac{\partial v^*}{\partial y^*} = 0 \quad (1)$$

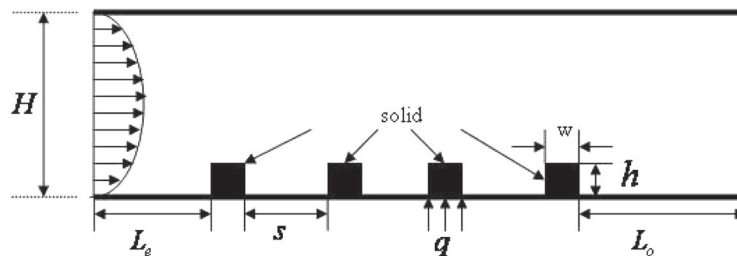


Figure 1. Schematic diagram of the forced convective cooling of an array of obstacles.

$$\text{Re}_H \left( u^* \frac{\partial u^*}{\partial x^*} + v^* \frac{\partial u^*}{\partial y^*} \right) = -\frac{\partial p^*}{\partial x^*} + \left( \frac{\partial^2 u^*}{\partial x^{*2}} + \frac{\partial^2 u^*}{\partial y^{*2}} \right) \quad (2)$$

$$\text{Re}_H \left( u^* \frac{\partial v^*}{\partial x^*} + v^* \frac{\partial v^*}{\partial y^*} \right) = -\frac{\partial p^*}{\partial y^*} + \left( \frac{\partial^2 v^*}{\partial x^{*2}} + \frac{\partial^2 v^*}{\partial y^{*2}} \right) \quad (3)$$

$$\text{Pe}_H \left( u^* \frac{\partial \Theta_f}{\partial x^*} + v^* \frac{\partial \Theta_f}{\partial y^*} \right) = \frac{\partial^2 \Theta_f}{\partial x^{*2}} + \frac{\partial^2 \Theta_f}{\partial y^{*2}} \quad (4)$$

The energy equation for the solid blocks is

$$\left( \frac{k_s}{k_f} \right) \left( \frac{\partial^2 \Theta_s}{\partial x^{*2}} + \frac{\partial^2 \Theta_s}{\partial y^{*2}} \right) + \mathcal{Q} = 0 \quad (5)$$

where  $\mathcal{Q} = 0$  if a surface heat flux is supplied and  $\mathcal{Q} = 1$  if the heat is generated inside the obstacle. Consistent with results of Young and Vafai [6], it was found that the heating method did not have much effect on the Nusselt number. As such, in this work  $\mathcal{Q} = 0$  was adopted. The nondimensionalized variables used in Eqs. (1–5) are

$$\begin{aligned} u^* &\equiv \frac{u}{u_m} & v^* &\equiv \frac{v}{v_m} & x^* &\equiv \frac{x}{H} & y^* &\equiv \frac{y}{H} & p^* &\equiv \frac{pH}{\mu_f u_m} \\ \Theta &\equiv \frac{T - T_e}{qH/k_f} & \text{Re}_H &\equiv \frac{\rho_f u_m H}{\mu_f} & \text{Pe}_H &\equiv \frac{\rho_f c_p u_m H}{k_f} \end{aligned} \quad (6)$$

where  $u_m = H^{-1} \int_0^H u dy$  is the mean velocity and  $h^* \equiv \frac{h}{H}$ ,  $w^* \equiv \frac{w}{H}$ , and  $s^* \equiv \frac{s}{H}$  are nondimensionalized obstacle height, width, and spacing, respectively. The local Nusselt number is evaluated from

$$\text{Nu}_x = \frac{h_c H}{k_f} = -\frac{1}{\Theta_w} \frac{\partial \Theta_f}{\partial \vec{n}} \quad (7)$$

where the temperature gradient is obtained by using a three-point finite-difference scheme. The mean values of Nusselt numbers for each surface and overall Nusselt number are calculated using the following expressions:

$$\overline{\text{Nu}}_m = \frac{\int A_i \text{Nu}_x dx}{A_i} \quad (8)$$

$$\overline{\text{Nu}}_m = \frac{\sum_{i=L,T,R} \overline{\text{Nu}}_i A_i}{A_L + A_T + A_R} \quad (9)$$

where  $A_i$  is the area of the obstacle and the subscripts  $L$ ,  $T$ , and  $R$  indicate the left, right, or top face.

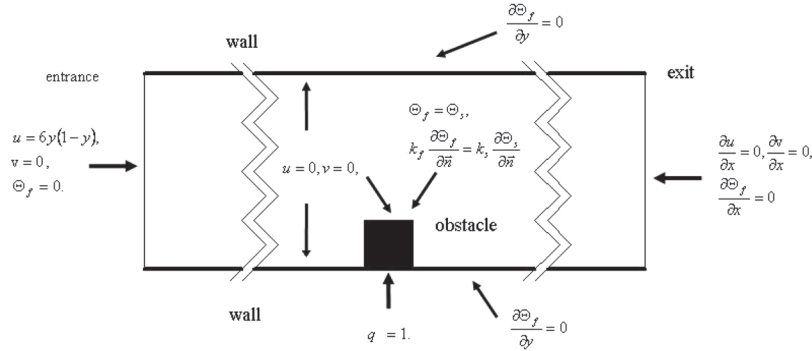


Figure 2. Schematic of the boundary conditions for different subdomains.

2.1. Boundary Conditions

Figure 2 shows the boundary conditions on different subdomains. At the entrance section, the flow is characterized by fully developed and parabolic profile. The temperature at the inlet is set to be equal to the ambient temperature.

$$u = 6y(1 - y) \quad v = 0 \quad \Theta_f = 0 \tag{10}$$

At the exit cross-section, the temperature and velocity gradient, and velocity gradient are both set equal to zero. This produces a less restrictive exit boundary condition.

$$\frac{\partial u}{\partial x} = 0 \quad \frac{\partial v}{\partial x} = 0 \quad \frac{\partial \Theta_f}{\partial x} = 0 \tag{11}$$

At the bottom of each solid domain a uniform heat flux is applied. At the interfaces between the air and the solid obstacles, the no-slip condition and the continuity of temperature and heat flux are applied.

$$u = 0 \quad v = 0 \quad \Theta_f = \Theta_s \quad k_f \frac{\partial \Theta_f}{\partial \vec{n}} = k_s \frac{\partial \Theta_s}{\partial \vec{n}} \tag{12}$$

Finally, the upper and lower channel walls which are exposed to the flow are considered as insulated surfaces. This results in

$$u = 0 \quad v = 0 \quad \frac{\partial \Theta_f}{\partial y} = 0 \tag{13}$$

3. RESULTS AND DISCUSSION

Four sets of comparisons were conducted to assess and establish the accuracy of the numerical results. First, the local Nusselt number distribution along the

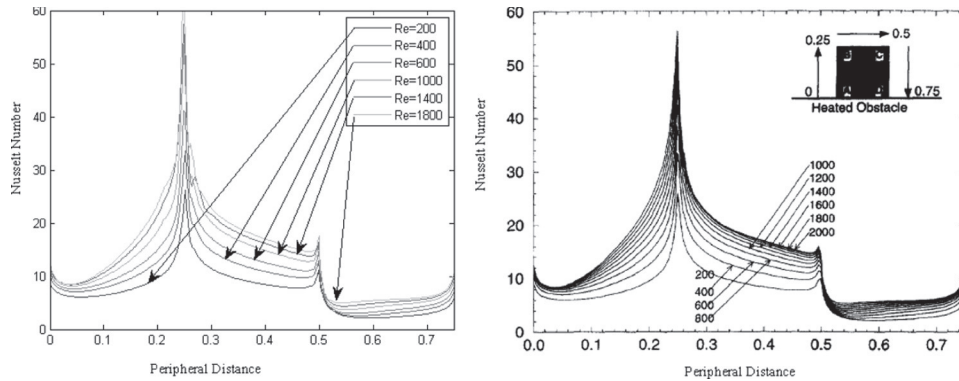


**Figure 3.** Comparison of the local Nusselt number along the left top, and right faces of an obstacle with the result of Young and Vafai [5] (RHS) for a single obstacle with  $q_w = 1,200 \leq Re_{Dh} \leq 2,000$ ,  $w = 0.25$ , and  $h = 0.25$ .

surfaces of a single obstacle was compared with the results of Young and Vafai [5]. The comparison is shown in Figure 3. There is an excellent agreement between these results. Along the left surface ( $0 \rightarrow 0.25$ ), the Nusselt number reaches the local minimum before rising up. This happens close to the edge, as the incoming flow impinges on the front surface of the obstacle and creates a vortex. Heat dissipated away from the front surface recirculates inside this vortex, causing the heat transfer coefficient to decrease. Above the recirculation zone, the increase in upstream momentum causes the heat transfer coefficient to increase rapidly towards the upper corner. Along the top surface ( $0.25 \rightarrow 0.5$ ) the Nusselt number drops as the boundary grows. The convection from the back surface ( $0.5 \rightarrow 0.75$ ) is somewhat suppressed

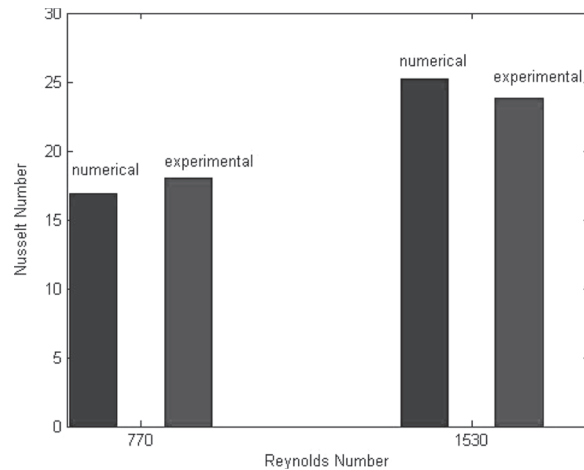


**Figure 4.** Comparison between the current numerical results and experimental data from Young and Vafai [4] for  $h/w = 0.89$ ,  $H/w = 3.11$ , and  $q = 930 \text{ W/m}^2$ .

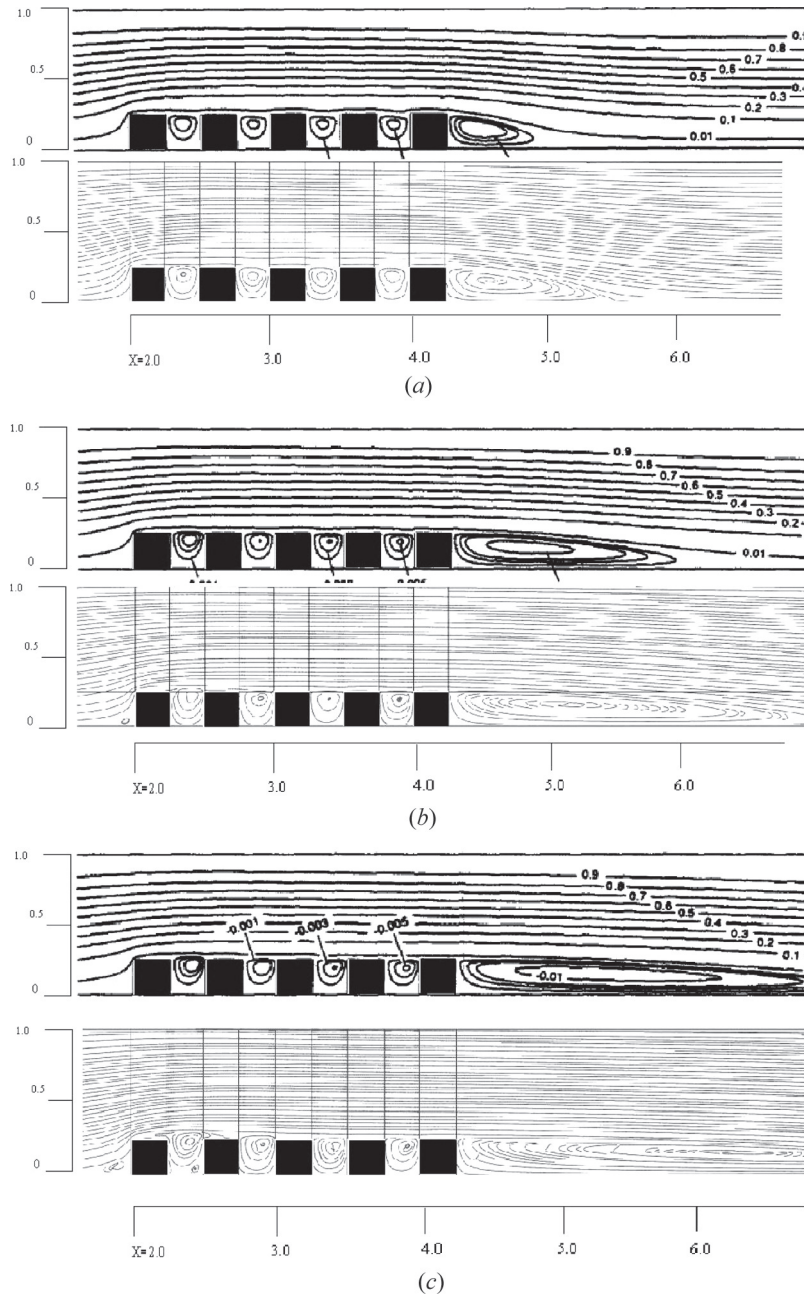


**Figure 5.** Comparison of streamlines between the present numerical results (lower) and the results of Young and Vafai [6] (upper) for a channel with five obstacles:  $w=0.25$ ,  $h=0.25$ , and  $s=0.25$ : (a)  $Re_{Dh}=200$ , (b)  $Re_{Dh}=800$ , and (c)  $Re_{Dh}=2,000$ .

compared to the other two surfaces due to the wake formed behind the back surface, which acts as an insulation layer.

The second comparison is done with the experimental data of Young and Vafai [4] for a single obstacle with height-to-width ratio of 0.89, channel height-to-width ratio of 3.11, and a  $930 \text{ W/m}^2$  input heat flux. Comparisons were done for  $\text{Re}_{Dh} = 770$  and  $\text{Re}_{Dh} = 1530$ . Figure 4 shows the comparison between the present numerical data and the experimental results. The results match quite well.

For an array of multiple obstacles mounted on a surface, two additional comparisons were made. The first one was for streamlines at different Reynolds numbers. The results from the current numerical resolution are compared to those produced by Young and Vafai [6], as shown in Figure 5. The flow produces a small downward pressure over the cavity as it passes over obstacles. As such, the vortices within the cavities are not able to rise over the top surface of the obstacle. The wake zone behind the leeward surface of the last obstacle is flattened and stretched further at higher Reynolds numbers. The results compare very well with a minor discrepancy with respect to the elongated size of the downstream wake for the current numerical results. This discrepancy is mainly due to the limited plotting options available in COMSOL which is the software that was used to generate the present results. To properly display the streamlines for the present results a more refined resolution of the streamlines had to be adopted. This created a denser looking recirculation zone.

The overall mean Nusselt number for each of the 10 identical obstacles at five different Reynolds numbers were also compared with the results of Young and Vafai [6].

As seen in Figure 6a,  $\overline{\text{Nu}}_m$  drops sharply from the first obstacle to the second one and declines smoothly for the following obstacles. The first obstacle benefits from the incoming flow impingement, thus it has the largest  $\overline{\text{Nu}}_m$ . The subsequent obstacles have lower  $\overline{\text{Nu}}_m$  due to lack of active interaction between the cavity vortex and the primary bypass flow as well as the growth of the thermal boundary layer over the top surfaces of the obstacles. For example, the difference between the value of  $\overline{\text{Nu}}_m$  for the ninth and the eighth obstacles is found to be within 4% for

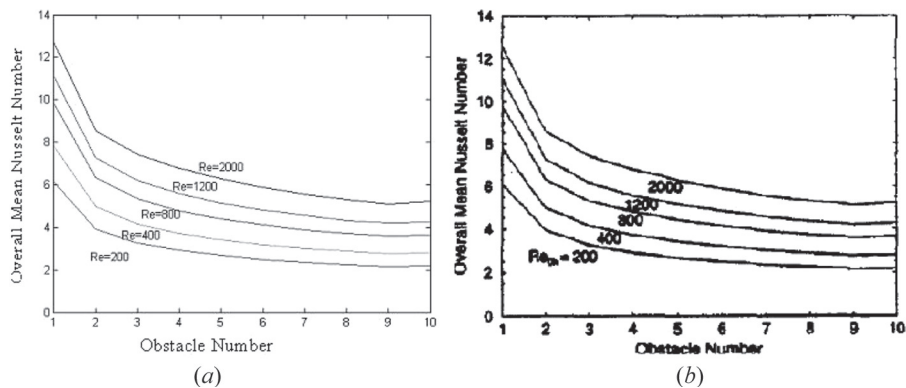


**Figure 6.** Overall mean Nusselt number for 10 identical obstacles at  $\text{Re} = 200, 400, 800, 1,200,$  and  $2,000$ . (a) Present results and (b) results from Young and Vafai [6].



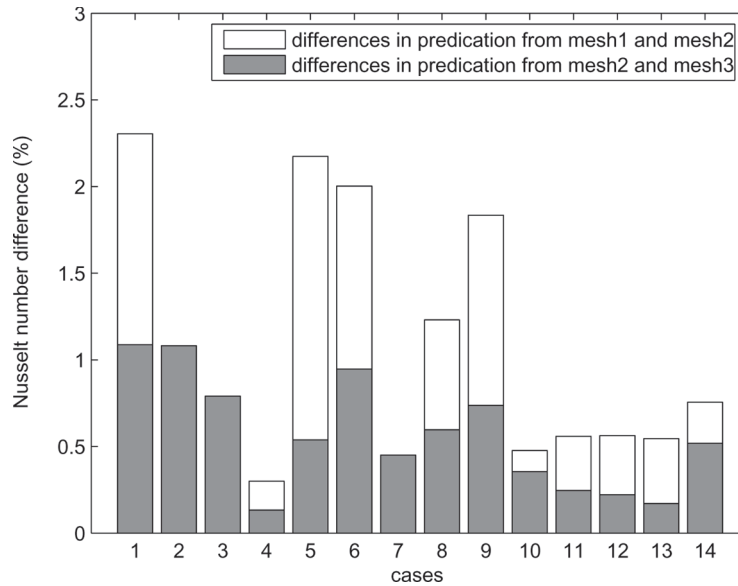


**Figure 7.** Differences among the most dense mesh, mesh 3, finer mesh, mesh 2, coarse mesh, and mesh 1, which were analyzed in this work.

$Re_{Dh} = 200$  and  $Re_{Dh} = 2,000$ . For obstacle seven, this difference is within 9%. The investigation of thermal periodicity conducted by Young and Vafai [6] is also presented in Figure 6b. The above cited differences are within 5% and 10% for the same conditions, respectively.

In this work, three types of mesh were applied to various geometrical domains, ranging from  $275 \times 45(x \times y)$  to  $555 \times 75(x \times y)$ . The grid independence studies are shown in Figure 7 for the three different mesh sizes. These were mesh 1:  $275 \times 45(x \times y)$ ; mesh 2:  $400 \times 600(x \times y)$ , and mesh 3:  $555 \times 75(x \times y)$ . As it can be seen in Figure 7, the largest difference between mesh 1 and mesh 2 is less than 2.5% and the difference between mesh 2 and mesh 3 is about 1%. As such due to extremely large number of computational runs, mesh 2 was chosen for the results produced in this work.















#### 4. EFFECTS OF PERTINENT PARAMETERS

Table 1 lists 14 basic cases, which when taken together present a thorough synthesis of various geometrical configurations related to placements of chips on a board. All of the pertinent geometrical effects were analyzed and taken into account in obtaining the correlations given in this work.

##### 4.1. Effect of Channel Height-to-Element Length Ratio

Clearance height to element length ratio  $(H - h)/w$  was reported to be one of those geometric parameters which had a substantial effect on the Nusselt number [4, 5]. The effect of this geometrical parameter on  $\overline{Nu}_m$  is presented in Figure 8. As expected, obstacles with larger channel height-to-element length ratio result in

Table 1. Cases which are examined in this work

Case	Graphic configuration	Width	Height	Spacing
1		0.25	0.25	0.25
2		0.125	0.125	0.375
3		0.25	0.125	0.25
4		0.5	0.125	0.25
5		0.125	0.25	0.5
6		0.25	0.25	0.5
7		0.125	0.125	0.5
8		0.5	0.25	0.25
9		0.125	0.25	0.375
10		0.5	0.125	0.5
11		0.25	0.125	0.375
12		0.25	0.125	0.5
13		0.5	0.125	0.375
14		0.375	0.25	0.5

a larger  $\overline{Nu}_m$ . As the Reynolds number increases, the influence of channel height-to-element length ratio on  $\overline{Nu}_m$  is amplified.

#### 4.2. Effect of Spacing-to-Channel Height Ratio

Spacing-to-channel height ratio,  $s/H$ , is another influential geometric parameter that affects  $\overline{Nu}_m$  [5]. The effect of spacing-to-channel height ratio is displayed in Figure 9. As this ratio increases, a wider space between the obstacles becomes available. As a result, the core flow enters the cavity more easily and mixes with vortices resulting in more heat removal. Case 6 has a larger spacing-to-channel height ratio compared to case 1. As expected, obstacles in case 6 have a larger value of  $\overline{Nu}_m$  compared to case 1.

#### 4.3. Effect of the Thermal Conductivity Ratio

The results from Young and Vafai [6] show little variations in  $\overline{Nu}_m$  when thermal conductivity ratio varies from  $k_s/k_f=10$  to 1,000. As such the effect of thermal conductivity ratio is considered to be small.

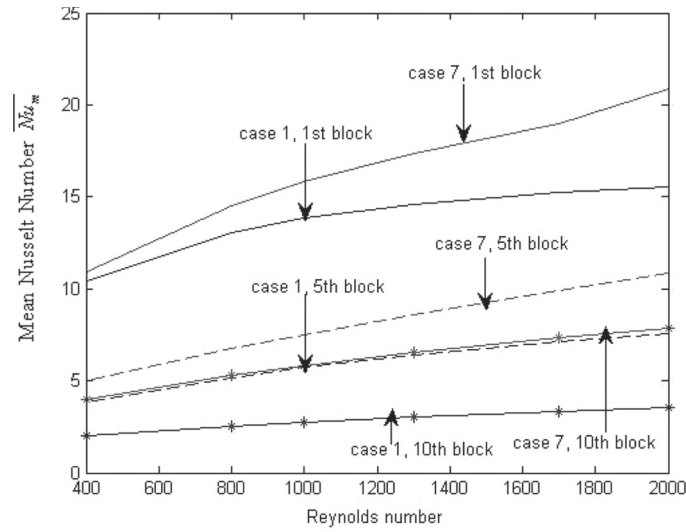


Figure 8. Effect of channel clearance height-to-element length ratio on overall mean Nusselt number: Case 1:  $(H-h)/w=3$  and case 7:  $(H-h)/w=7$ .

4.4. Effect of the Obstacle’s Geometric Ratio

Figure 10, displays the effect of a chip’s geometric ratio,  $h/w$ , on the average Nusselt number,  $\overline{Nu}_m$ . In general, the slender-taller obstacles produce a larger  $\overline{Nu}_m$  compared to a flatter-shorter obstacle for  $Re_{Dh} \leq 1,500$ . The only exception to this behavior is for the first block for  $Re_{Dh} > 1,500$ . When  $Re_{Dh} > 1,500$ , the  $\overline{Nu}_m$  is larger

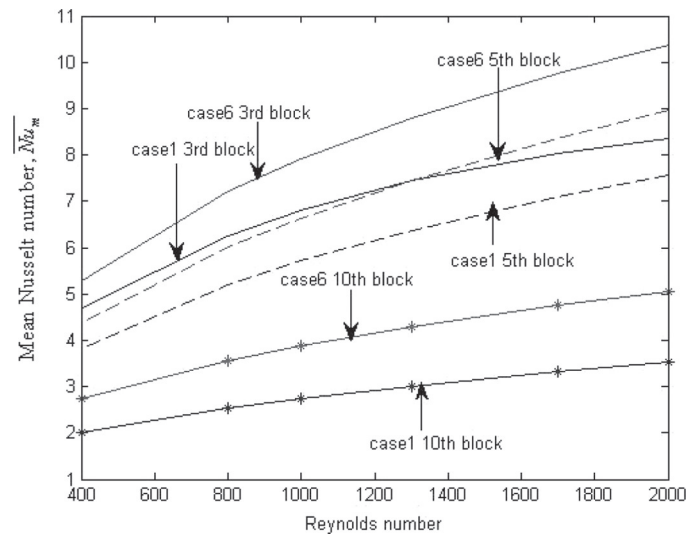


Figure 9. Effect of spacing-to-channel height ratio,  $s/H$ , on  $\overline{Nu}_m$  for cases 1 and 6.

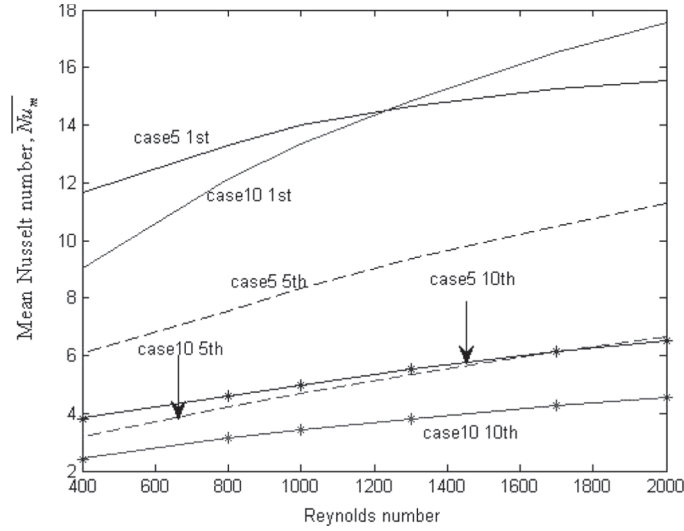


Figure 10. Effect of the obstacle’s geometric ratio,  $h/w$ , on  $\overline{Nu}_m$  for cases 5 and 10.

for the flatter-shorter first obstacle. This is due to the inverse influences from boundary layer development and vortices near the mounting edge. For lower Reynolds numbers, the first slender-taller obstacle benefits from incoming flow impingement. At the same time, the boundary layer is relatively thicker for lower Reynolds numbers. The thicker boundary layer diminishes the heat transport into the core flow. As the Reynolds number increases, the boundary layer becomes thinner while the vortex formed close to the mounting edge of the front surface gains strength and acts as an

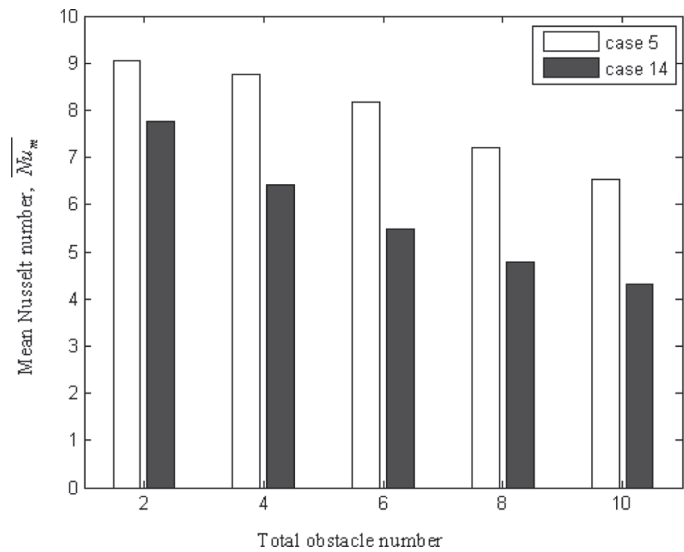


Figure 11. Effects of total obstacle numbers on  $\overline{Nu}_m$  for the last for  $Re_{Dh} = 2,000$ .

insulator. Consequently, the slender-taller first obstacle which mainly benefits from the impinging flow experiences a loss as the Reynolds number increases. By contrast, larger Reynolds numbers cause an increase in  $\overline{Nu}_m$  for the flatter-shorter first obstacle.

#### 4.5. Effect of the Total Number of Obstacles

The total number of obstacles affects the value of  $\overline{Nu}_m$ . The further an obstacle is located from the inlet, the smaller the value of  $\overline{Nu}_m$  will be due to the boundary layer growth. Also, since overall mean temperature of the bypass flow increases it becomes more difficult to transfer heat from the latter obstacles to the flow field. As seen in Figure 11, there is a clear decreasing trend line for  $\overline{Nu}_m$  over the last obstacle.

### 5. COMPREHENSIVE CORRELATION

After an exhaustive number of computational simulations, a comprehensive correlation which incorporates various geometrical attributes of the discussed array of blocks was obtained. This correlation is given by

$$\overline{Nu}_m = c_0 \text{Re}^{c_1} \left(\frac{s}{H}\right)^{c_2} \left(\frac{H-h}{w}\right)^{c_3} \left(\frac{h}{w}\right)^{c_4} N^{c_5} n^{c_6} \quad (14)$$

where  $c_0$  through  $c_6$  are constants, Re, the Reynolds number,  $s/H$  spacing-to-channel height ratio,  $(H-h)/w$ , channel height-to-element length ratio,  $h/w$  geometric ratio of the blocks,  $N$  total number of obstacles, and  $n$  is the obstacle number.

This comprehensive correlation was based on a very large number of numerical runs. The coefficients for this correlation are given in Table 2. Note that exponent  $c_1$  for Reynolds number and the exponent  $c_6$  for the obstacle number in Eq. (14) are close to 0.5 and  $-0.5$ , respectively, which correspond to some extent to the thermal entry boundary layer development in a channel when the obstacles are considered to be much shorter than the channel height. The range of applicability of this correlation is for  $200 \leq \text{Re}_{Dh} \leq 2,000$ ;  $2 \leq N \leq 10$ ;  $1/4 \leq h/w \leq 2$ ;  $0.25 \leq s/H < 0.5$ , and  $0.5 < (H-h)/w < 7$ . It should be noted that comprehensive details and physical

**Table 2.** Correlation coefficients and average error

Coefficient	1st obstacle	2nd–10th obstacles	All obstacles
$c_0$	0.8377	0.4376	0.5364
$c_1$	0.3458	0.4377	0.4224
$c_2$	-0.0644	0.2555	0.2022
$c_3$	0.2480	0.2736	0.2693
$c_4$	-0.1291	0.0582	0.0270
$c_5$	0.0049	0.1032	0.0891
$c_6$	0	-0.4529	-0.5321
Error against all of the numerical simulation data	$\pm 4.06\%$	$\pm 6.71\%$	$\pm 9.36\%$

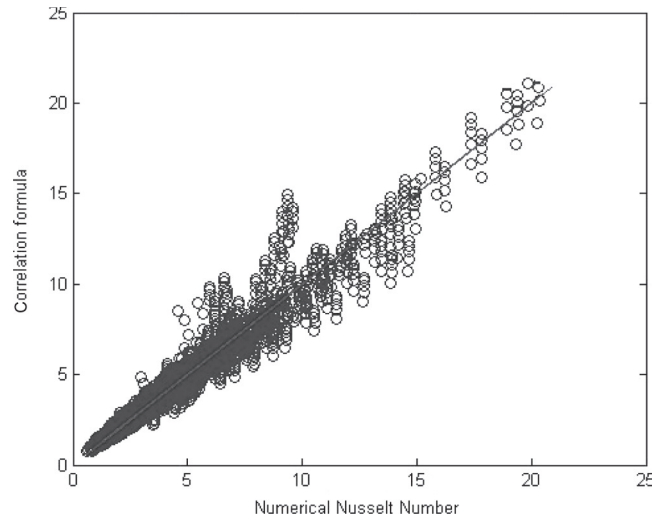


Figure 12. Comparison of the single tier correlation against the actual numerical data.

attributes for the case when there is only one obstacle is given in Young and Vafai [5]. Figure 12 displays predictions from Eq. (14) against the actual numerical simulation data. The average error between the actual data and Eq. (14) is  $\pm 9.36\%$ . Most of the scatter is related to the first obstacle. As mentioned before,  $\overline{Nu}_m$  experiences a sharp decline when flow passes from the first obstacle to the second. This trend suggests adaptation of another strategy to produce a more accurate correlation. This strategy is based on using a two tier correlation, one for the first obstacle and another, respectively, for blocks 2–10. The corresponding coefficients for this two tier correlation are

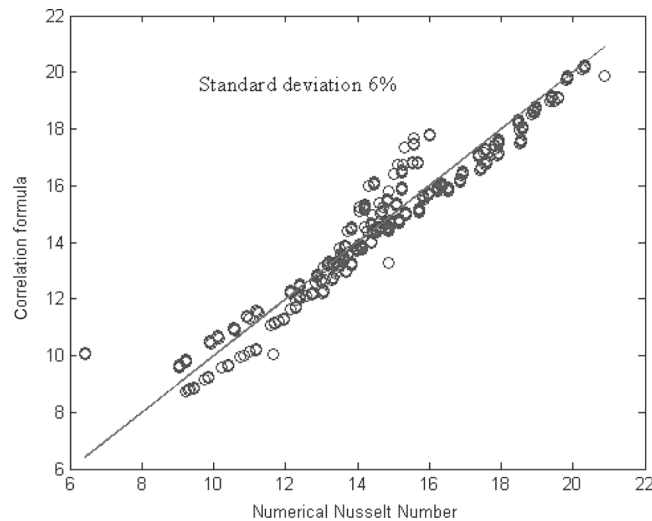
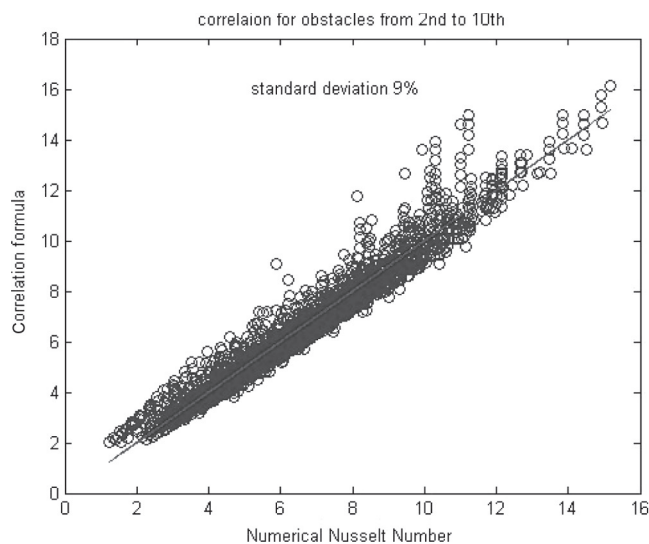


Figure 13. Comparison of the correlation for the first block with the actual numerical data.



**Figure 14.** Comparison of the correlation for the 2nd–10th obstacles with the actual numerical data.

given in Table 2 and the comparisons with the actual computational data are given in Figures 13 and 14. As it can be seen there is a better match with the data for the two tier correlation, with average error of  $\pm 4.06\%$  and  $\pm 6.71\%$  for the first block and the remaining blocks correlations, respectively.

## 6. CONCLUSION

A comprehensive correlation representing convective cooling of an array of obstacles and incorporating various pertinent geometrical arrangements such as channel clearance height-to-element length ratio, geometric ratio of the obstacles, spacing-to-channel height ratio, and the total number of blocks as well as the Reynolds number is established in this work. This correlation is based a very large number of simulations. Very good agreement was found when the numerical results presented in this work were compared against works for single and multiple obstacles.

Several pertinent physical attributes for an array of obstacles were discussed. The comprehensive correlation using only a single equation representation yielded an average error of  $\pm 9\%$  against all of the numerical simulation data. A two equation correlation was also established for the first and all the remaining obstacles, respectively. This two tier correlation yielded an average error of  $\pm 4\%$  for the first obstacle and  $\pm 7\%$  for the remaining obstacles.

## REFERENCES

1. E. R. Meinders and K. Hanjalic, Vortex Structure and Heat Transfer in Turbulent Flow over a Wall-Mounted Matrix of Cubes, *Int. J. of Heat and Fluid Flow*, vol. 20, pp. 255–267, 1999.

2. S. V. Garimella and P. A. Eibeck, Heat Transfer Characteristics of an Array of Protruding Elements in Single Phase Forced Convection, *Int. J. Heat and Mass Transfer*, vol. 33, no. 12, pp. 2659–2669, 1990.
3. G. K. Morris and S. V. Garimella, Composite Correlations for Convective Heat Transfer from Arrays of Three-Dimensional Obstacles, *Int. J. Heat and Mass Transfer*, vol. 40, no. 2, pp. 493–498, 1997.
4. T. J. Young and K. Vafai, Experimental and Numerical Investigation of Forced Convective Characteristics of Arrays of Channel Mounted Obstacles, *J. Heat Transfer*, vol. 121, no. 1, p. 34, 1999.
5. T. J. Young and K. Vafai, Convective Cooling of a Heated Obstacle in a Channel, *Int. J. Heat and Mass Transfer*, vol. 41, pp. 3131–3148, 1998.
6. T. J. Young and K. Vafai, Convective Flow and Heat Transfer in a Channel Containing Multiple Heated Obstacles, *Int. J. Heat and Mass Transfer*, vol. 41, pp. 3279–3298, 1998.
7. A. Korichi and L. Oufer, Unsteady Heat Transfer and Pressure Drop in Channels with Obstacles Mounted on the Upper and Lower Walls, *Numer. Heat Transfer A*, vol. 48, no. 7, pp. 711–729, 2005.
8. C. W. Leung, S. Chen, and T. L. Chan, Numerical Simulation of Laminar Forced Convection in an Air-Cooled Horizontal Printed Circuit Board Assembly, *Numer. Heat Transfer A*, vol. 37, no. 4, pp. 373–393, 2000.
9. T.-H. Hsu, P.-T. Hsu, and S.-P. How, Mixed Convection in a Partially Divided Rectangular Enclosure, *Numer. Heat Transfer A*, vol. 31, no. 6, pp. 655–683, 1997.
10. T. J. Heindel, S. Ramadhyani, and F. P. Incropera, Conjugate Natural Convection from an Array of Protruding Heat Sources, *Numer. Heat Transfer A*, vol. 29, no. 1, pp. 1–18, 1996.
11. P. C. Huang and K. Vafai, Internal Heat Transfer Augmentation in a Channel Using an Alternate Set of Porous Cavity-Block Obstacles, *Numer. Heat Transfer A*, vol. 25, no. 5, pp. 519–539, 1994.
12. C.-I. Baek, K.-S. Lee, and W.-S. Kim, Study of Combined Heat Transfer in a Three-Dimensional Enclosure with a Protruding Heat Source, *Numer. Heat Transfer A*, vol. 32, no. 7, pp. 733–747, 1997.
13. M. Keyhani, L. Chen, and D. R. Pitts, The Aspect Ratio Effect on Natural Convection in an Enclosure with Protruding Heat Sources, *Trans. of the ASME, J. of Heat Transfer*, vol. 113, no. 4, pp. 883–891, 1991.
14. N. Yuçel and R. T. Guven, Forced-Convection Cooling Enhancement of Heated Elements in a Parallel-Plate Channels using Porous Inserts, *Numer. Heat Transfer A*, vol. 51, no. 3, pp. 293–312, 2007.
15. U.S. Department of Defense, Reliability Prediction of Electronic Equipment, Military Handbook MIL-HDBK-217 F, chap. 6, Washington, D.C., 1991.